POLYTECHNIQUE MONTRÉAL

Stage en laboratoire

Laboratory for Multiscale Mechanics

Numerical evaluation of periodic forcing influence in the Fluid Mechanical Sewing Machine problem

Yago Pego Martínez
Matricule : 2036204

Content Index

1. Introduction

The goal of this bachelor thesis is to carry on with the study of the behavior of liquid ropes and its thin viscous jet instabilities, as previously done by *Brun et al*. (see Ref. [1]) and other professionals. This coiling and folding phenomenon of a viscous stream onto a surface can be reproduced in a simple yet well-controlled experiment, where a viscous thread is deposited on a moving belt: the patterns laid down by the thread are diverse and include meandering, alternating and coiling loops. The resemblance of these patterns to the stitch patterns of a sewing machine led Ref. [2] to call the system the "fluid mechanical sewing machine" (FMSM). Similar coiling patterns can be found in everyday situations, such as the production of non-woven textiles or the laying down of "squiggles" of icing on cakes. Some patterns produce evenly spaced self-intersection which can serve as sacrificial bonds [3-4]: solified fibers containing such a microstructure display a combination of high toughness and stretchability revealed by mechanical tests, as they effectively reproduce nature's design for spider silk.

While we will firstly introduce the original, standard geometrical model which we would often see in previous papers [1,5], the aim of this project is to evaluate the influence of a new external kinematic forcing; that is, the implementation of a sinusoidal-like movement for the extruding head point.

Pattern eventuality observed in the new geometrical model will prove to be essentially equivalent to the one studied in the original FMSM problem, maintaining common morphological and parametric characteristics.

This all will lead to the real core of the project, which consists on the statistical and Fourier frequency characterization of each of the considered patterns, along with the said external forcing. An equivalent analysis has been previously done by *Jawed et al* [5], on the standard model, and will thus serve as a comparative figure for the result analysis.

It is to be said that this presumably constitutes the first attempt to model and characterize the kinematics of an externally forced FMSM problem.
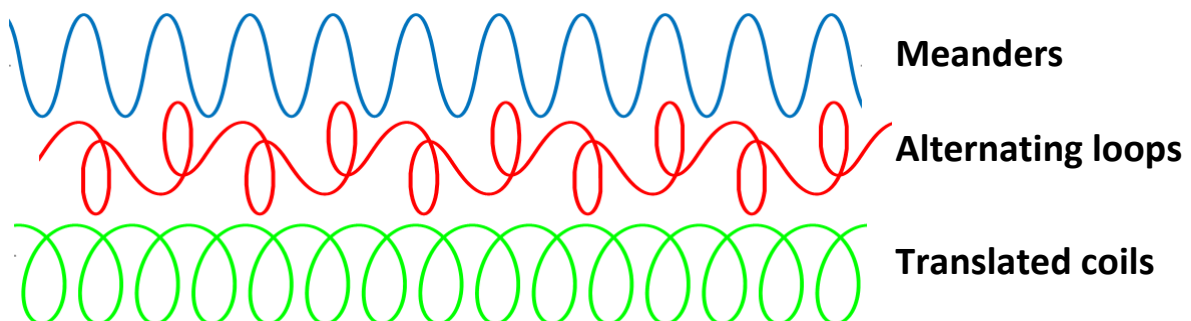

Meanders

Alternating loops

Translated coils

Figure 1. FMSM primary patterns.

2. Physics of the new geometrical model

We pursue to understand the instabilities derived from the implementation of a sinusoidal movement on the 3D-printing nozzle. Our geometrical model is based on the one described in the scientific paper *Liquid Ropes: A Geometrical Model for Thin Viscous Jet Instabilities* (Brun et al, 2015 [1]).
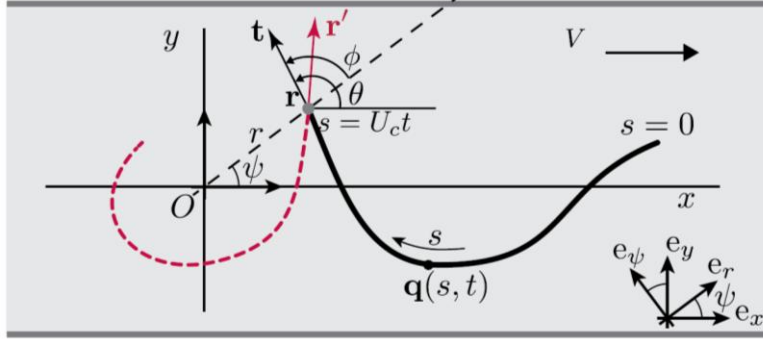

Figure 2. Standard geometrical model. (*Brun et al*, 2015 [1]).

The model above represents, in the plane of the belt where the thread is deposited, the trace q (thick black curve) with arc length s, orbit of the contact point (dashed red curve), and projection O of the nozzle onto the belt's plane. The curvature of the thread is assumed to be a function of the polar coordinates (r, ϕ) of the point of contact r.

$$U_c t + V\, e_x = \dot{r} \tag{1}$$

where U_c is defined as the steady coiling speed, determined by the steady coiling frequency, f_c, and radius, R_c, while V is the belt speed, a constant.

Let $q(s, t)$ be the position on the belt of the point s at time t, with $0 \leq s \leq U_c t$. This point was deposited at time s/U_c at position $r(s)$, and it has subsequently been advected at velocity $V\, e_x$ by the belt. Thus:

$$q(s, t) = r(s) + V\left(t - \frac{s}{U_c}\right) e_x \tag{2}$$

To further extend our research, as mentioned above, we have thought of introducing a sinusoidal transverse perturbation. Let A be the amplitude of the movement, and T, the period of the sine wave, the perturbation is defined as:

$$Y(t) = A \sin\left(2\pi \frac{t}{T}\right) \tag{3}$$

Since s is defined as the arc length along the deposited trace, it seems natural to have the deposited trace within one wavelength named, for instance, λ. Now, given that $\lambda = U_c T$ and $s = U_c t$, it is possible to express the sinusoidal perturbation in terms of the arc length s:

$$Y(s) = A \sin\left(2\pi \frac{s}{\lambda}\right) \tag{4}$$

4

Adding this to the general equations on (1) and (2), we obtain the following updated expressions:

$$U_c \boldsymbol{t} + V\, \boldsymbol{e}_x + \dot{Y}\, \boldsymbol{e}_y = \dot{\boldsymbol{r}} \tag{5}$$

$$\boldsymbol{q}(s,t) = \boldsymbol{r}(s) + V\left(t - \frac{s}{U_c}\right)\boldsymbol{e}_x + Y(s)\boldsymbol{e}_y \tag{6}$$

The definition of the origin O in our new problem changes with respect to the one used in Figure 2. O is no longer the projection of the nozzle onto the belt's plane, but rather the specific projection of the nozzle over the movement's unique middle point ($O{:}\,Y = 0$).

The tangent to the trace $\boldsymbol{t} = \partial\boldsymbol{q}/\partial s$ is now:

$$\boldsymbol{t} = \frac{\partial \boldsymbol{q}}{\partial s} = \boldsymbol{r}'(s) - \frac{V}{U_c}\boldsymbol{e}_x + Y'(s)\,\boldsymbol{e}_y \tag{7}$$

where $Y'(s) = \frac{2\pi A}{\lambda}\cos\left(2\pi\frac{s}{\lambda}\right)$.

Prior to continuing, let us establish the correspondence between the Cartesian and polar basis:

$$\begin{Bmatrix}\boldsymbol{e}_x \\ \boldsymbol{e}_y\end{Bmatrix} = \begin{bmatrix}\cos\psi & -\sin\psi \\ \sin\psi & \cos\psi\end{bmatrix}\begin{Bmatrix}\boldsymbol{e}_r \\ \boldsymbol{e}_\psi\end{Bmatrix} \tag{8}$$

The tangent vector $\boldsymbol{t}$ can be expressed in the polar basis:

$$\boldsymbol{t} = \cos\phi\,\boldsymbol{e}_r + \sin\phi\,\boldsymbol{e}_\psi \tag{9}$$

Now, we recover Eq. (5) with $\boldsymbol{r}' = \dot{\boldsymbol{r}}/U_c$. Let $\big(r(s), \psi(s)\big)$ denote the polar coordinates of the contact point $\boldsymbol{r}(s)$, as shown in Figure 2, and let $\theta(s)$ denote the angle from the x-axis to $\boldsymbol{t}(s)$. We resolve $\boldsymbol{r}', Y', \boldsymbol{t}, \boldsymbol{e}_x$ and $\boldsymbol{e}_y$ into the polar basis $(\boldsymbol{e}_r, \boldsymbol{e}_\psi)$ and use $\phi = \theta - \psi$ to eliminate the dependence on ϕ:

$$r' = \cos(\theta - \psi) + \frac{V}{U_c}\cos\psi - \frac{2\pi A}{\lambda}\cos\left(2\pi\frac{s}{\lambda}\right)\sin\psi \tag{10a}$$

$$r\psi' = \sin(\theta - \psi) - \frac{V}{U_c}\sin\psi - \frac{2\pi A}{\lambda}\cos\left(2\pi\frac{s}{\lambda}\right)\cos\psi \tag{10b}$$

Finally, θ' is the curvature of the trace at the contact point in terms of a fitting function[1]:

$$\theta' = \kappa(r, \theta - \psi) \tag{10c}$$

Equations $(10a) - (10c)$ are a set of coupled ordinary non-linear differential equations for the functions $r = r(s)$, $\psi = \psi(s)$ and $\theta = \theta(s)$, depending on a dimensionless parameter V/U_c, the wave amplitude A and the wave arc length λ. We refer to this system of equations as the new *geometrical model* (NGM). The kinematic equations $(10a)$ and $(10b)$ capture the coupling with the moving belt, while Eq. $(10c)$ captures the shape of the hanging thread as set by the balance of viscous forces and gravity.

We integrated the NGM numerically, varying the speed ratio $(SR = U_c/V)$, the frequency ratio $(FR = f_y/f_p)$ and the length ratio $(LR = A/R_c)$. These last two parameters are a novelty with respect to the standard approach, but they seem the best way to interpret the intricacies of the newly posed problem. Making the intrinsic variables $(f_c, R_c, U_c(f_c, R_c))$ in each quotient equal to a standard value, it is possible to test different scenarios by varying these unique three ratio-parameters involved.

A note on the frequency ratio will be added in the following chapter.

3. Pattern eventuality

As introduced in previous parts of the project, pattern eventuality in the FMSM problem becomes primarily dependent on the speed ratio defined, that is, the quotient between the extruding speed and the belt speed.

Noticeable speed-ratio intervals appear for each of the mentioned patterns, let us remember: meandering, alternating and coiling patterns. These are known as the primary patterns in related literature [5].

We provide the reader with a brief presentation of the said morphological patterns, in the traditional FMSM-problem frame of reference.

The following figures show the deposited trace for several speed-ratio scenarios. Both x- and y-axes are normalized by the steady coiling radius: $\widetilde{X} = x/R_c$ and $\widetilde{Y} = y/R_c$.
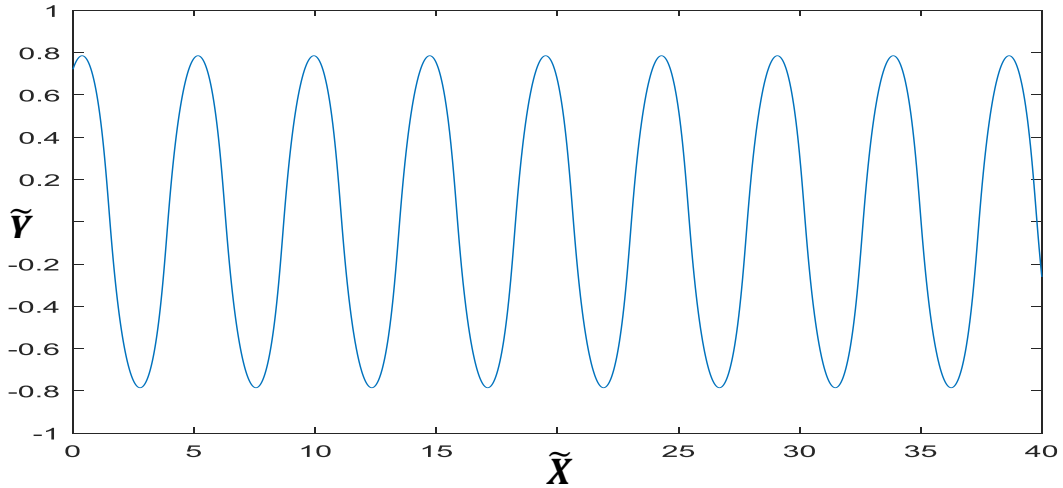

Figure 3. Plot of deposited trace for $SR = 1.25$. Meandering pattern.

The meandering pattern is to be found in the interval $SR \in (1.05, 1.40)$, when our arbitrary input variables are $R_c = 1$ and $f_c = 1$. It was found that the interval would slightly broaden when R_c was augmented, but these intricacies will, however, be declared beyond the scope of this project. The limiting case, where $SR = 1$, makes for a straight line over the moving belt, as expected.
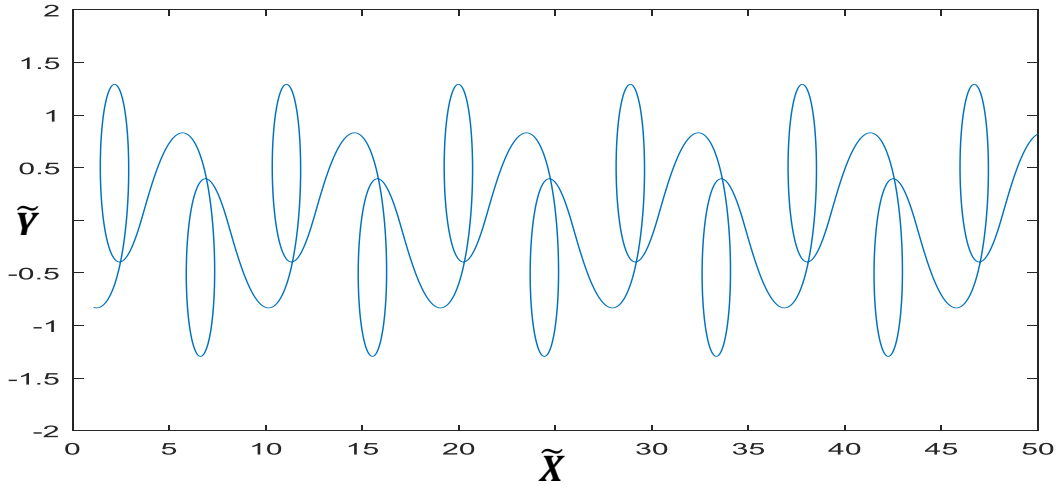
Figure 4. Plot of deposited trace for $SR = 2.2$. Alternating pattern.

The alternating pattern covered the interval $SR \in (1.85, 2.7)$.
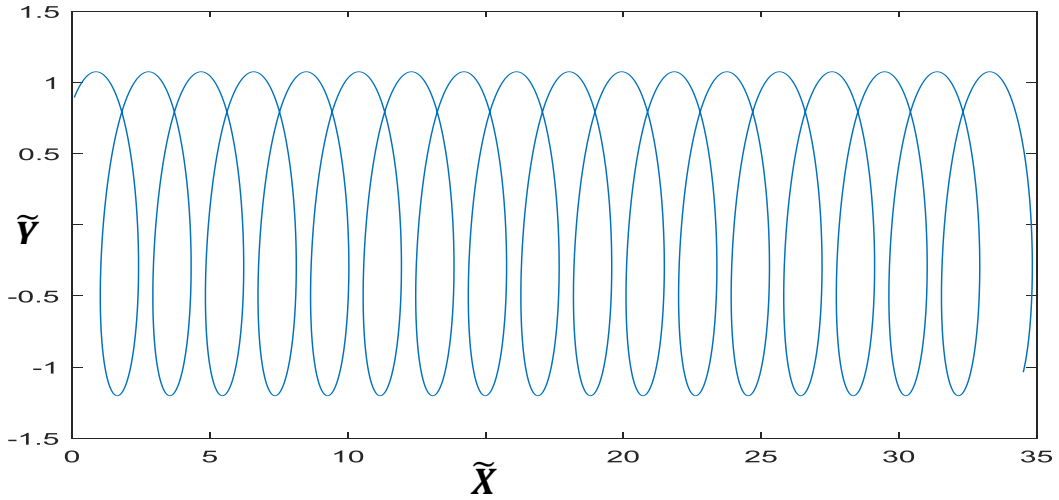

Figure 5. Plot of deposited trace for $SR = 3.8$. Coiling pattern.

Lastly, the coiling pattern will appear for speed ratios greater than $SR = 3.4$. A subtle differentiation has been made in previous literature between the coiling pattern and the overlapping pattern [3], the last one being a subtype of the first one, characterized by the superposition of one edge of the loop over the next one. For simplicity purposes, these last two patterns will be treated as one, since this will not interfere in future analyses.

Intermediate speed-ratio intervals are left for secondary or transitional patterns, which will not be considered in this project. For further information on these, see Ref. [5].

In what follows, we identify the distinguishing features of each pattern based on its frequency spectrum. In particular, we focus on the peak frequencies, denoted as $\overline{f}{}_x^{\,i}$ and $\overline{f}{}_y^{\,i}$ for the longitudinal and transverse directions, respectively, where the integer i is the order of the peak in increasing sequence, e.g., $\overline{f}{}_x^{\,1}$ is the first frequency along the longitudinal direction. The ratio of the amplitudes for the spectra for $\overline{f}{}_x^{\,i}$ and $\overline{f}{}_y^{\,i}$, denoted as A^i, will also be considered [5].

These frequencies on the horizontal axis have been normalized by the steady coiling frequency $f_c = U_c/(2\pi R_c)$. Amplitude has also been normalized by the maximum global amplitude seen. With respect to the plot of the contact point trace on the upper-left corner, equal axes have been adopted, making for a more precise amplitude visualization.
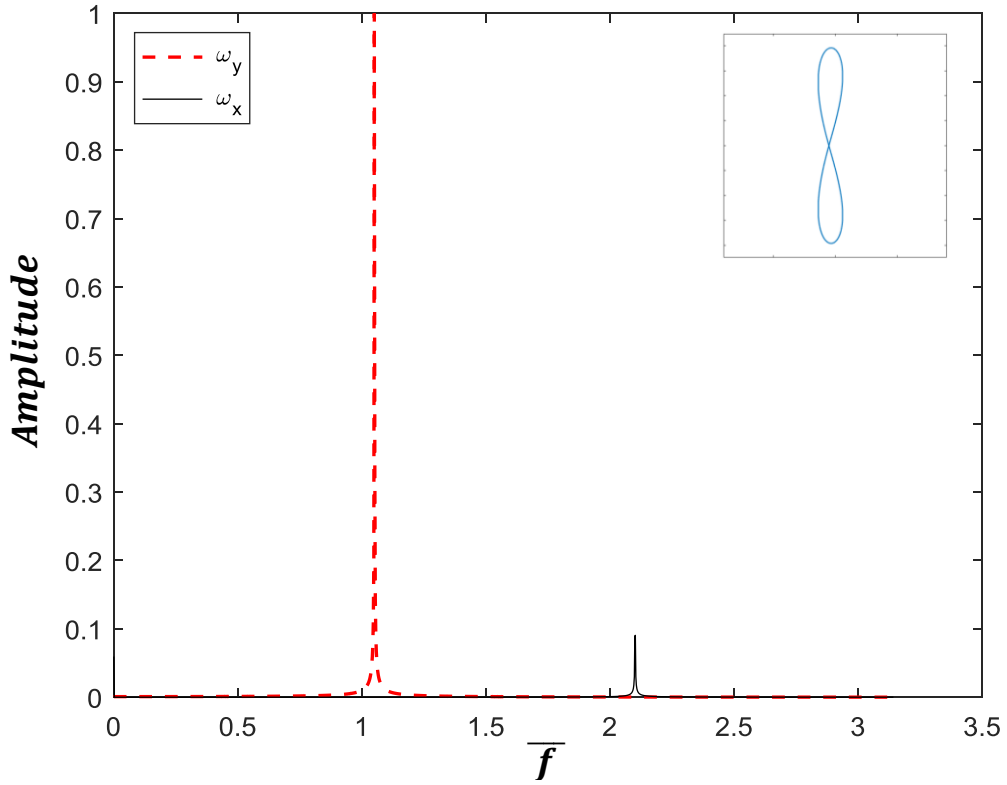
Meandering pattern

Figure 6. FFT diagram and contact point trace plot –top left– for $SR = 1.25$. Meandering pattern.

Single frequency peaks are observed for each of the space coordinates. A linear relation is found between these peaks $\overline{f}{}_x^{\,1}/\overline{f}{}_y^{\,1} = 2$ and amplitude ratio is $A^1 \ll 1$. First frequency peak is $\overline{f}{}_y^{\,1} \approx 1.05$.
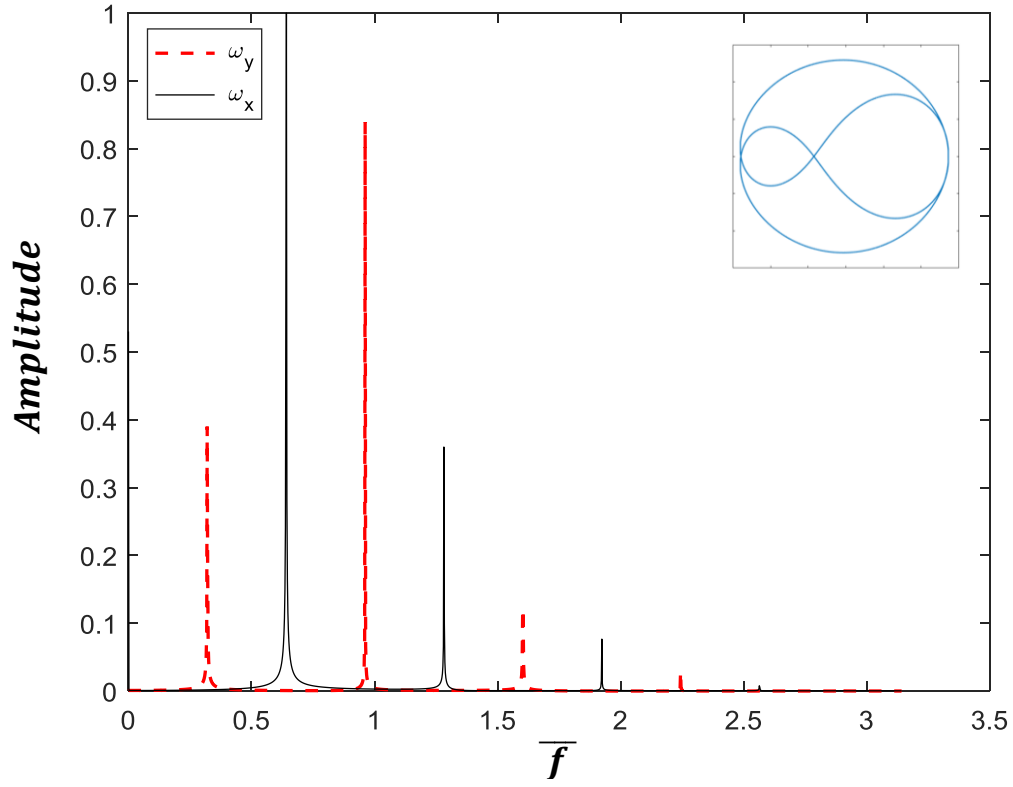
Figure 7. FFT diagram and contact point trace plot –top left– for $SR = 2.2$. Alternating pattern.

Several main frequency peaks arise, both in the longitudinal and transverse directions. They are, however, altogether related. y-axis frequencies are given by $\overline{f}_y^{\,i} = (2i - 1)\overline{f}_y^{\,1}$, while $\overline{f}_x^{\,i} = (2i)\overline{f}_y^{\,1}$, for $i = 1,2,3$. Amplitudes can be diverse. First frequency peak is $\overline{f}_y^{\,1} \approx 0.32$.
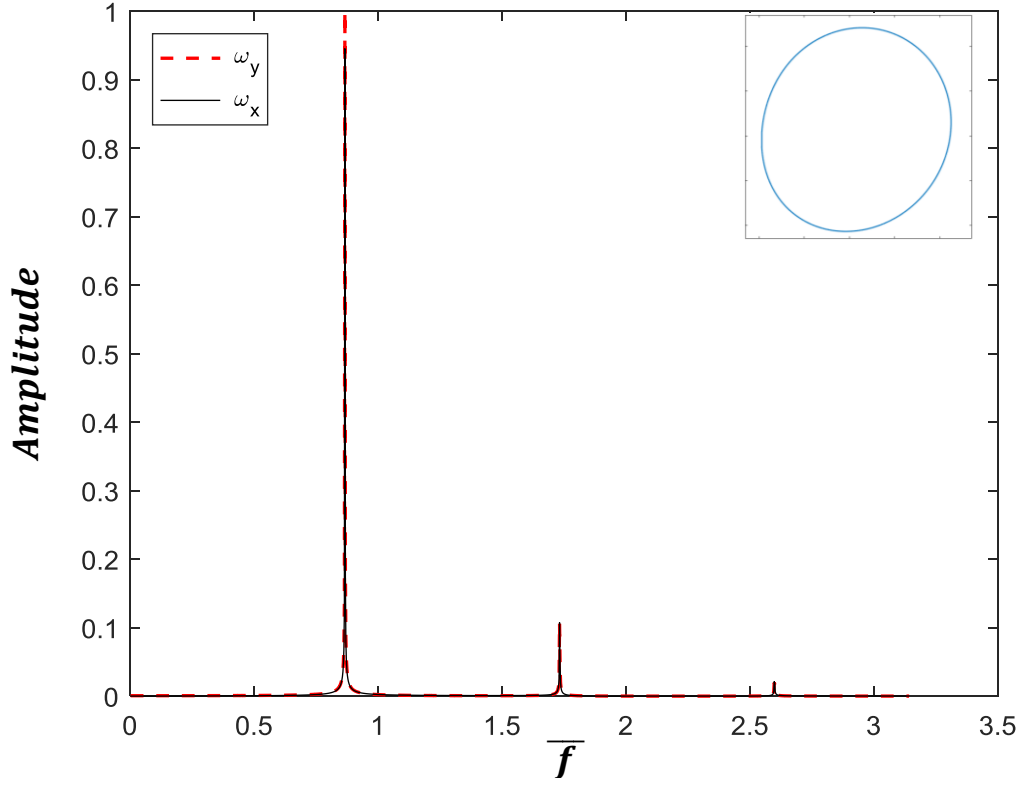
Coiling pattern

Figure 8. FFT diagram and contact point trace plot –top left– for $SR = 3.8$. Coiling pattern.

Lastly, translated coils give for a symmetrical frequency behavior. A principal frequency peak is found near the unity, while a secondary one stands on double the first value. Amplitudes are found equal, $A^i = 1$. The extreme case, one where $SR \gg 1$, corresponds to an almost static belt. Unique x and y frequencies with the same amplitude would be found at $\overline{f} = 1$. First frequency peak is $\overline{f}_y^1 \approx 0.87$.

Before delving into the numerical evaluation of the forcing scheme, a point has to be made regarding a finding in the Fourier frequency pattern characterization. To do so, let us imagine a recurring curvilinear pattern on a plane –contact point trace plots shown above may serve as an example. If we think of a circle, determining its cycle length, generally known as perimeter, is reduced to knowing its radius. If working with numerical software, we may even segment its trajectory in a small enough fashion so that we obtain a precise, equivalent sum of tiny element lengths.

Since an analytical expression does not exist for calculating, for instance, the cycle length of the alternating pattern in Figure 7; this last numerical method is employed to measure the total cycle length of a recurring pattern. In our example, this value translates to the total amount of material deposited within this cycle. If we now recall that arc length along the deposited trace, s, is proportional to time –seen before Eq. 4–; we realize that not only have we obtained the length ratio of that particular pattern and the steady circular pattern,

but this is also equal to the period ratio: $\lambda_p/\lambda_c = T_p/T_c$ (where the sub-index p stands for the particular pattern, and c stands for the steady coiling regime).

The inverse of this value, may we name it the primitive frequency ratio, $FR0$, appeared to correspond with the first y-axis normalized frequency on the FFT plot, $\overline{f}\,^1_y$. This realization can help us predict, by looking at the FFT plot, the total length of material expected to carry out a complete pattern cycle.

This last finding has proved to be a useful feature in the continuation of the project; when implementing the external forcing, to be more precise. As stated in the previous chapter, the choice of the frequency ratio $FR = f_y/f_p$ must be explained. f_y is defined as the perturbation frequency, while f_p represents the pattern frequency for a specific speed ratio in an unforced test, also given by $f_p = f_c\overline{f}\,^1_y$. The pattern frequency has been defined as the first main y-axis normalized frequency found on the FFT plot, times the original steady coiling frequency.

We can, however, expect this value to be highly dependent on the speed ratio: $\overline{f}\,^1_y \approx 0.3$ for $SR = 2.2$, or $\overline{f}\,^1_y \approx 1$ for $SR = 1.25$. In short, the new perturbation frequency f_y will be compared to the pattern frequency f_p, and not the originally introduced steady coiling frequency f_c. This model makes for a better understanding of the response of the system to the external forcing.

4. Statistical and frequency characterization of perturbed flow

It is in the LM2's (Laboratory for Multiscale Mechanics of École Polytechnique de Montréal) interest to get an insight into the response of small amplitude periodic perturbations with a frequency near the pattern's natural frequency.

4.1. Statistical analysis

In what follows, a series of externally forced experiments is compared to the one correspondent unforced simulation. x- and y-axes are unchanging (that is, the same for all sub-figures) and have both been normalized by the steady coiling radius, R_c, so they remain dimensionless.

Meandering pattern

Figure 9. Plot of deposited trace. Comparison of an unforced experiment with experiments with small forcing amplitude. Under pattern frequency forcing. Meandering pattern. $SR = 1.25 - FR = 0.9$.

Regarding the figure above, no major changes are perceived with respect to the unforced experiment, when the forcing frequency is slightly under the pattern frequency. It is arguable that, indeed, the experiment correctly responds to the new stimulation, since it maintains the original pattern.
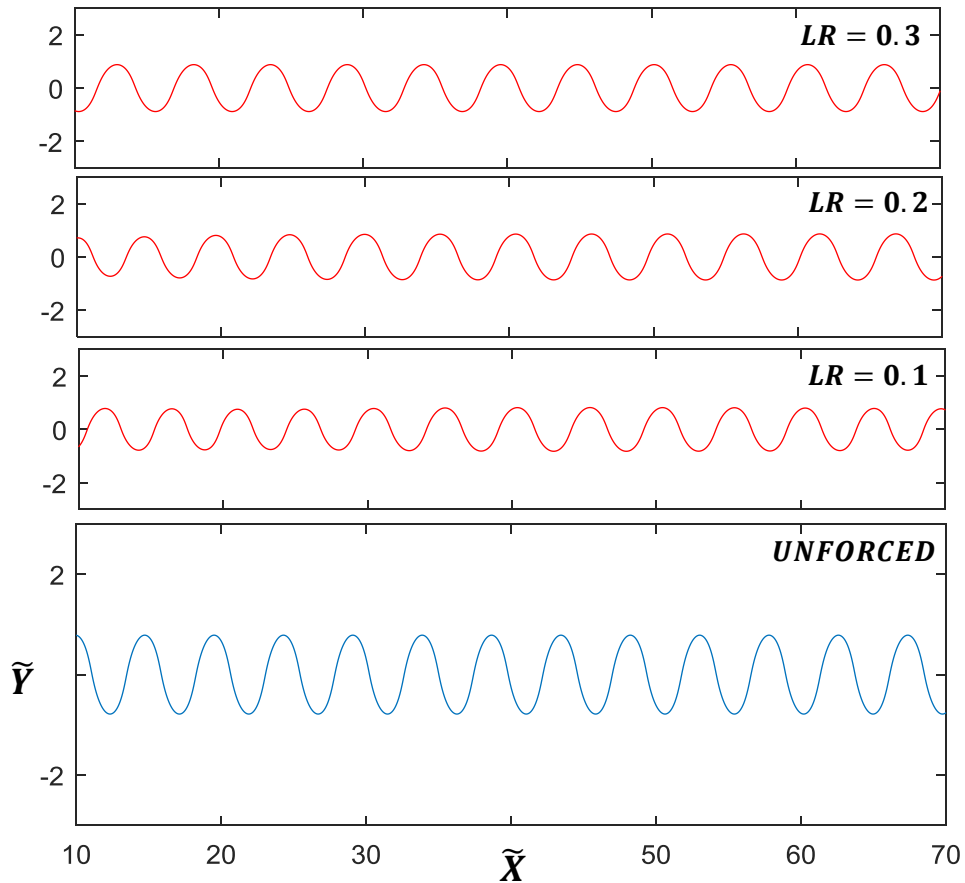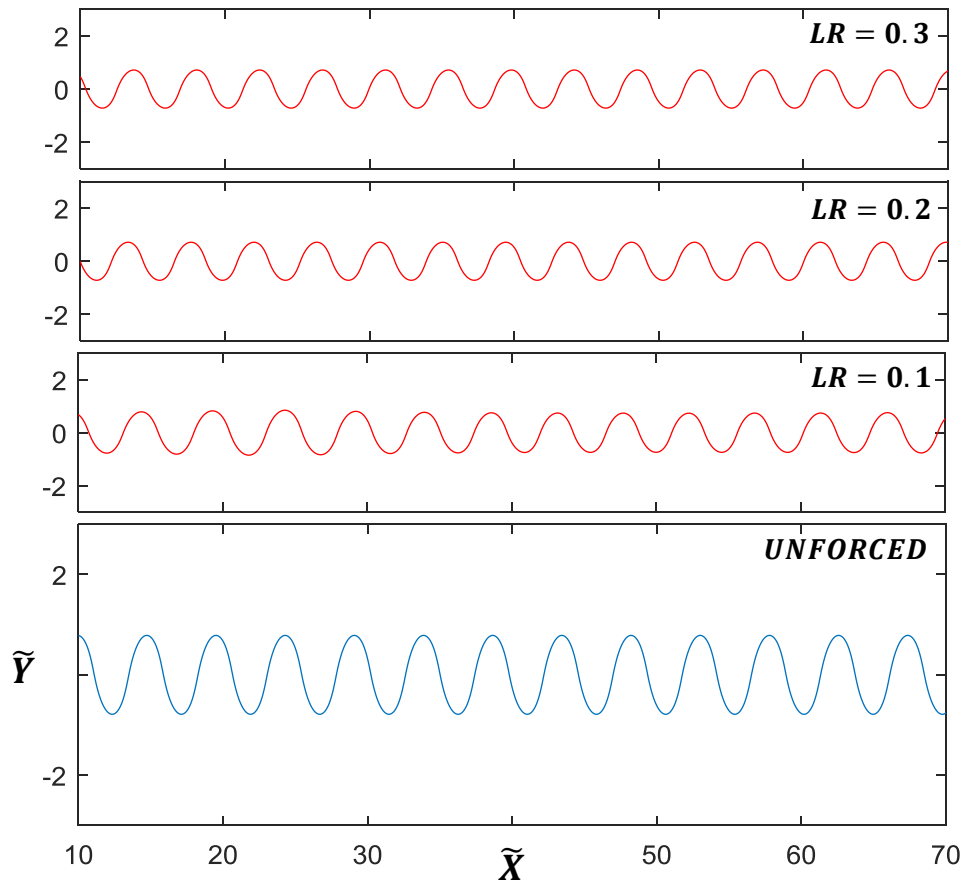
Figure 10. Plot of deposited trace. Comparison of an unforced experiment with experiments with small forcing amplitude. Above pattern frequency forcing. Meandering pattern. $SR = 1.25 - FR = 1.1$.

For the second meandering-pattern simulation, when the forcing frequency is slightly above the pattern frequency, results obtained are equally satisfactory. There is no evident detail that suggests a morphological variation in the experiments.

The following table illustrates more thoroughly the consequences of forcing implementation.

$SR = 1.25$	$|A|_{max}$				RMS		
Unforced	0.7853				0.5533		
	$FR = 0.9$	$FR = 1$	$FR = 1.1$		$FR = 0.9$	$FR = 1$	$FR = 1.1$
$LR = 0.1$	0.8206	0.7875	0.8526		0.5601	0.5539	0.5451
$LR = 0.2$	0.8664	0.7889	0.7148		0.5935	0.5541	0.5032
$LR = 0.3$	0.8786	0.7902	0.7161		0.6162	0.5544	0.5034

Table 1. Comparative study of experiment deviation. Meandering pattern.

The last table classifies the experiments carried out by its maximum normalized amplitude, $|A|_{max}$ –maximum deviation from the mean–, and its RMS (root-mean-standard). Some conclusions are to be taken from this table. First, behavior under pattern frequency ($FR = 0.9$) has provided some convincing results, where movement amplitude and RMS seem to naturally grow for greater amplitude forcings. Meanwhile, forcing at pattern frequency turned out to have almost no influence on pattern characterization. Lastly, above pattern frequency experiments, while visually unperceivable on Figure 10, resulted on smaller movement amplitude and RMS, when compared to the original experiment.

On another note, RMS value for the unforced experiment also has some insightful meaning. It is known that the RMS of a sine wave is 0.707 of its peak value. Our meandering counterpart has an $RMS = 0.5533$, which, divided by $|A|_{max}$, amounts to 0.705. This goes to show that the meandering pattern can be almost approximated by a sinusoidal wave. Another fact that supports this statement is the finding of the y-axis pattern frequency extremely close to the steady coiling frequency $(\overline{f}\,_y^{\,1} \rightarrow 1^+$, see Figure 6).

Alternating pattern

Figure 11. Plot of deposited trace. Comparison of an unforced experiment with experiments with small forcing amplitude. Under pattern frequency forcing. Alternating pattern. $SR = 2.2 - FR = 0.9$.

Once again, slightly under-pattern-frequency forcing responds visually well. In fact, there is no actual visual difference between the diverse experiments.
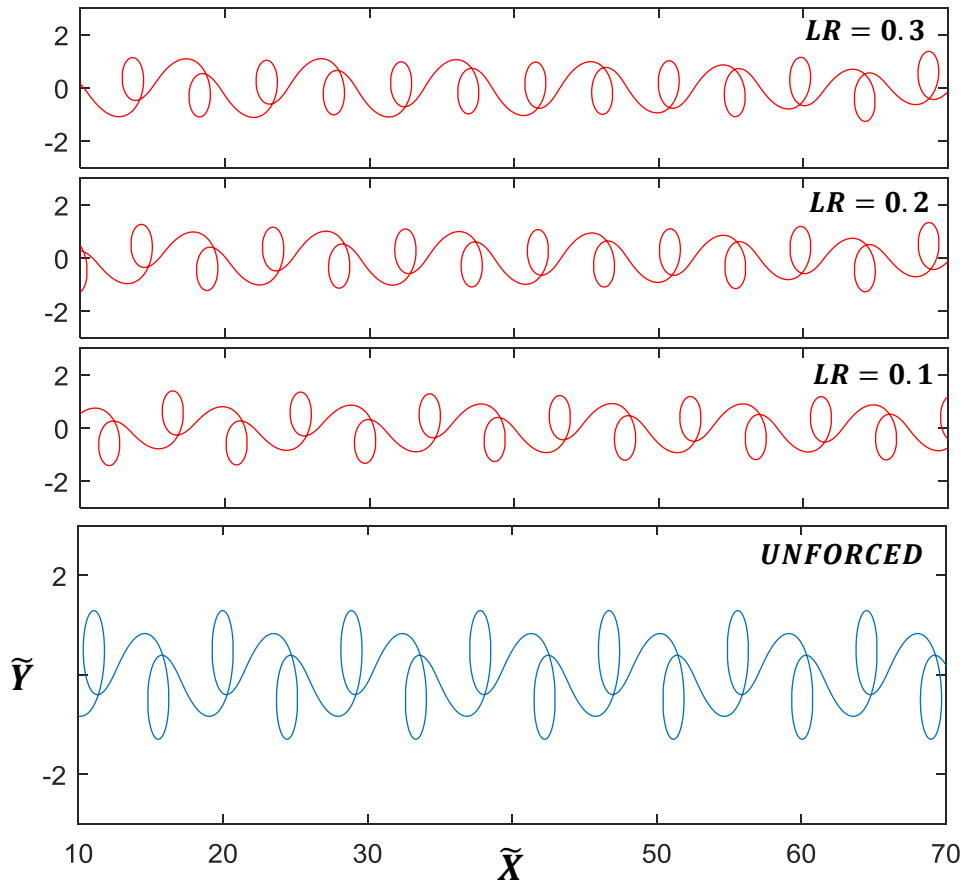

Figure 12. Plot of deposited trace. Comparison of an unforced experiment with experiments with small forcing amplitude. Above pattern frequency forcing. Alternating pattern. $SR = 2.2 - FR = 1.1$.

Same thing can be said for Figure 12. Alternating pattern has been barely affected by forcing frequencies near its natural frequency, neither when it is defined above it.

$SR = 2.2$	$|A|_{max}$				RMS		
$Unforced$	1.2926				0.6612		
	$FR = 0.9$	$FR = 1$	$FR = 1.1$		$FR = 0.9$	$FR = 1$	$FR = 1.1$
$LR = 0.1$	1.4080	1.2376	1.4181		0.6612	0.6408	0.6680
$LR = 0.2$	1.5296	1.2133	1.5510		0.6652	0.6280	0.6872
$LR = 0.3$	1.6521	1.2059	1.6921		0.6782	0.6207	0.7185

Table 2. Comparative study of experiment deviation. Alternating pattern.

Table 2 includes amplitude and RMS characterization for the unforced alternating pattern, as well as the forced experiments. Over 1 amplitude must be noted. This means that the thread is naturally deposited at a farther position than the own steady coiling radius, when the speed-ratio (between the extruding speed and the belt speed) is held at $SR \sim 2 - 3$. This is a novelty with respect to the meandering pattern, where normalized amplitude never surpassed the unity.

In short, slightly under- ($FR = 0.9$) and above- ($FR = 1.1$) pattern forcing frequencies offer intuitive and expected results, where amplitude and RMS accordingly grow. A point has to be made on the $FR = 1$ experiment (when forcing frequency is equal to pattern frequency). While counter-intuitive, amplitude shrinks, and so does RMS. An additional figure has not been added to showcase this, since form is quite unchanging.
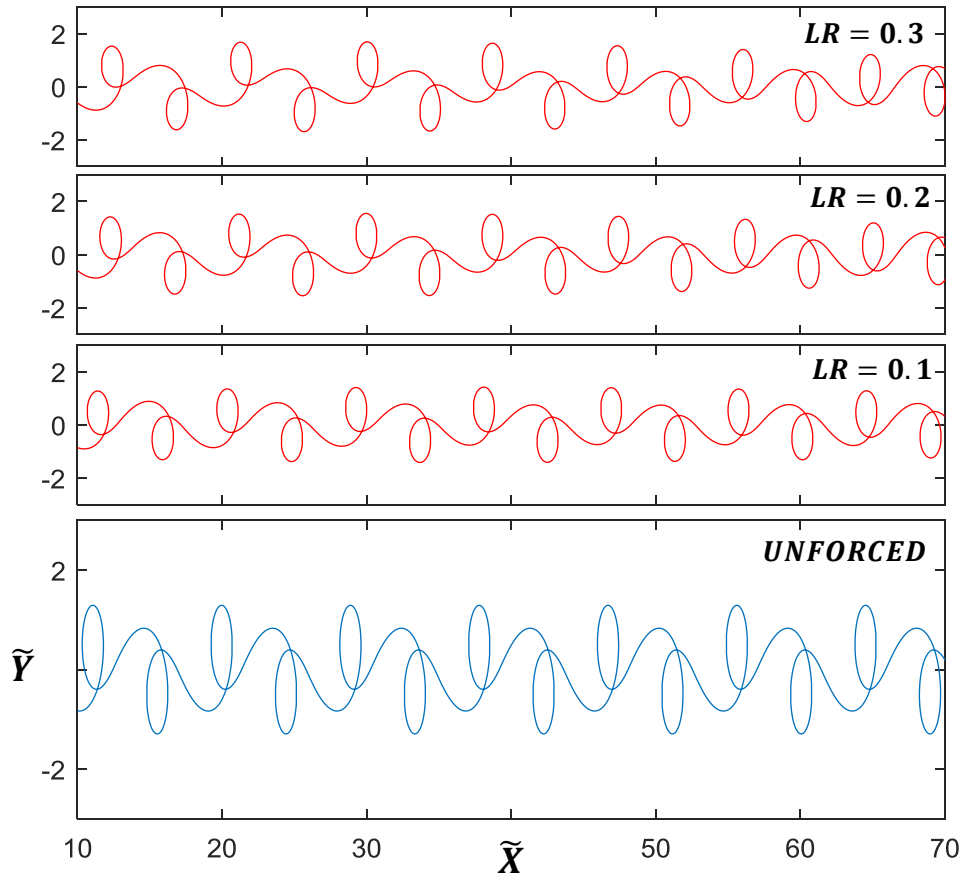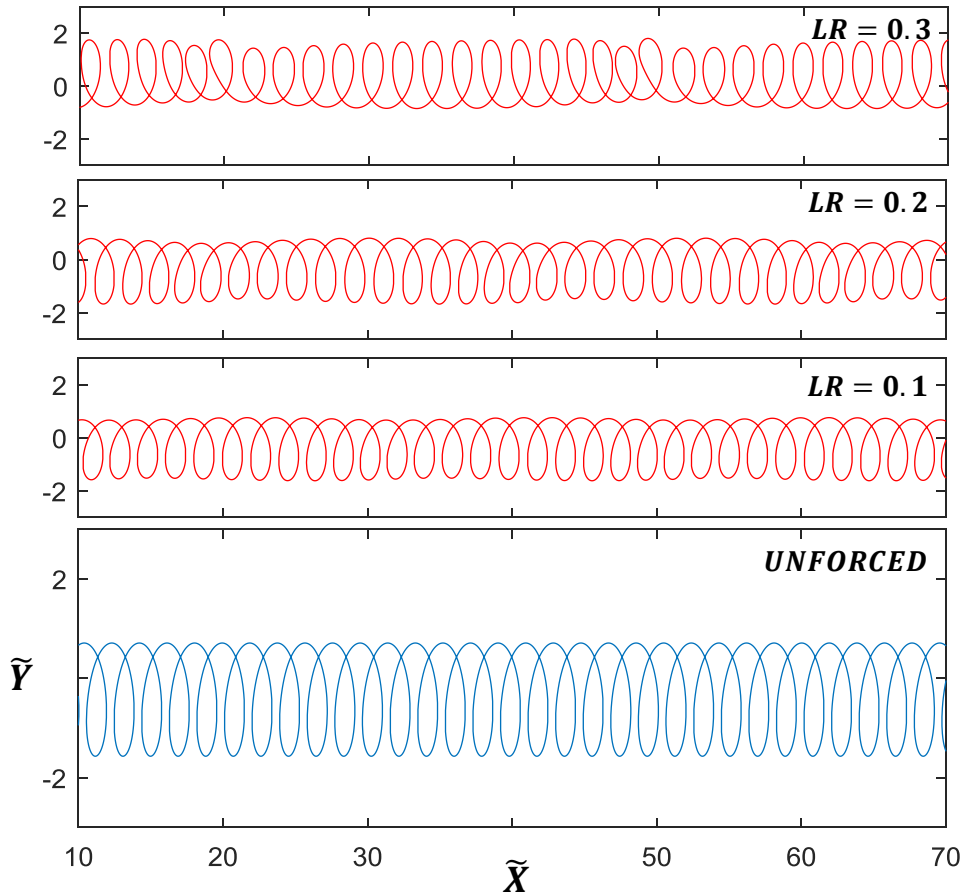
Coiling pattern

Figure 13. Plot of deposited trace. Comparison of an unforced experiment with experiments with small forcing amplitude. Under pattern frequency forcing. Coiling pattern. $SR = 3.8 - FR = 0.9$.

For the coiling pattern, instability is to be encountered when surpassing a length ratio (LR) of around 0.2. After that, coils may periodically enroll in heterogeneous behavior. For instance, the sense of loop formation has completely changed for the uppermost subfigure. To further insist on this, an additional figure is added below for an even higher length ratio.
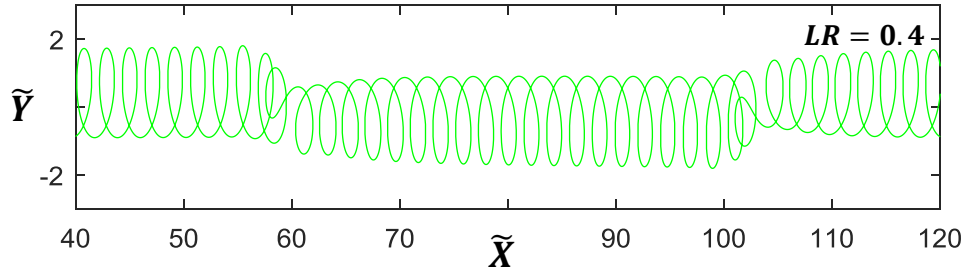
Figure 14. Plot of deposited trace. Forced experiment, under pattern frequency. Coiling pattern. $SR = 3.8 - FR = 0.9$.

As shown in the figure above, not only unconventional loops are periodically formed, but also the sense of the loop is not fixed. We may now confidently discard this type of simulations, as the coiling pattern is not consistent for relatively small amplitude forcings.
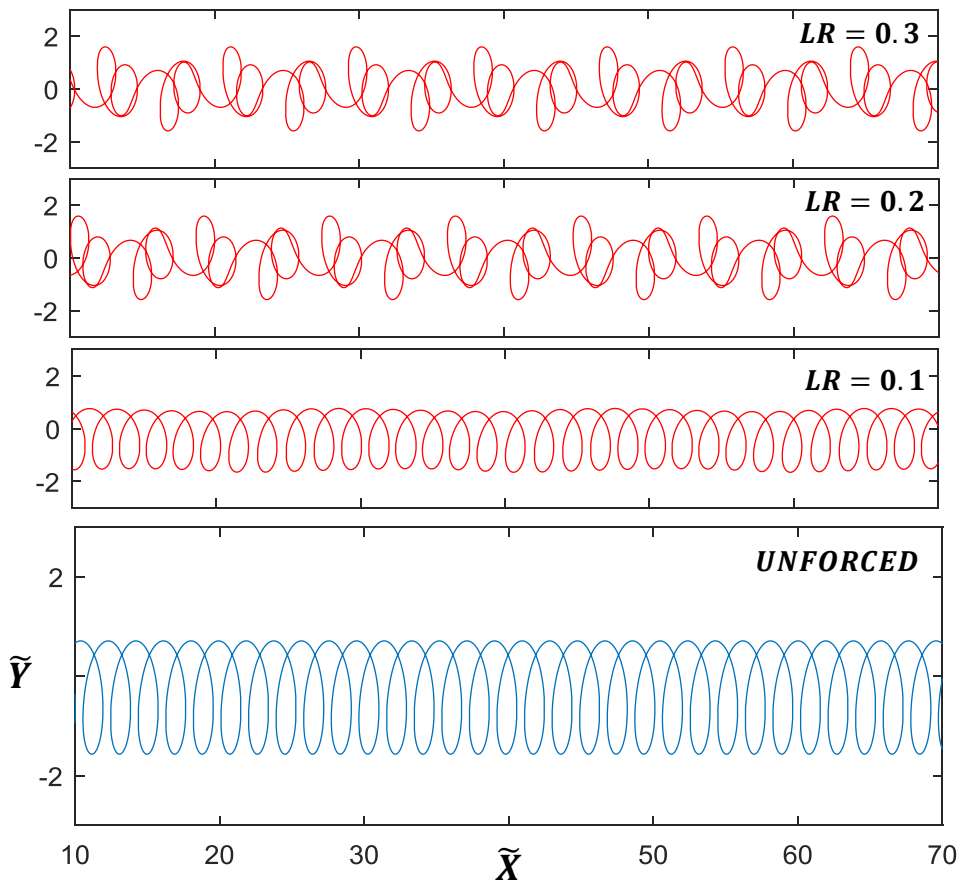
Figure 15. Plot of deposited trace. Comparison of an unforced experiment with experiments with small forcing amplitude. Above pattern frequency forcing. Coiling pattern. $SR = 3.8 - FR = 1.1$.

In Figure 15, once again instability is observed. Coiling pattern is no longer consistent for $LR > 0.1$. The results seen in the top subfigures do not share any morphological or periodic relation with the unforced example. Even larger length ratios accomplish nothing but even larger unstable and random loops.

Data in the table below corroborate how heterogeneous the results obtained are:

| $SR = 3.8$	$|A|_{max}$				RMS		
Unforced	0.9952				0.8383		
	$FR = 0.9$	$FR = 1$	$FR = 1.1$		$FR = 0.9$	$FR = 1$	$FR = 1.1$
$LR = 0.1$	1.0483	1.0125	1.0584		0.8428	0.8623	0.8435
$LR = 0.2$	1.0955	1.0152	1.5792		0.8561	0.8966	0.7582
$LR = 0.3$	1.4953	2.8972	1.5895		0.8823	0.9177	0.7607

Table 3. Comparative study of experiment deviation. Coiling pattern.

Before stating the obvious, a point can be made with regards to the unforced experiment amplitude. Its proximity to the unity implies that the amplitude of the pattern (a circle when projecting under the nozzle, to be more precise: see Figure 8) is almost equal to the steady coiling radius. On the bad side, as predicted by the graphs on the previous page, the coiling pattern becomes inconsistent soon, for relatively small forcing amplitudes.

4.2.   Frequency analysis

Frequency analysis has been done for particularly interesting variable-ratio combinations, as predicted by the statistical study. The methodology follows the one seen on Chapter 3: *Pattern eventuality*. A change is made, however, in the FFT diagrams. The spectrum of frequencies is now normalized by the pattern frequency (f_p), not the steady coiling frequency (f_c) anymore. This way, the results will look far more intuitive, now that a user-defined frequency ratio (FR) is part of the equation.

Figure 16. FFT diagram and contact point trace plot –top left– for a forced experiment. Under pattern frequency forcing. $SR = 1.25 - FR = 0.9 - LR = 0.3$.

The meandering pattern holds on quite well and a clean figure and spectrum of frequencies are obtained. The first y-axis frequency is found, unsurprisingly, at $\overline{f}_y^1 = 0.9$. Complying with the model in Figure 6, a second, smaller, frequency peak is observed at $\overline{f}_x^1 = 2\overline{f}_y^1$.

The diagram cleanliness, or lack of residual frequencies –they will be seen in following figures–, may be attributed to the fact that the meandering pattern has proved to be quite flexible regarding the point of appearance of its pattern frequency over an extended frequency interval. The implementation of near-pattern-frequency frequencies does not seem to disrupt its regular thread flow.

Same thing can be said for the simulation in Figure 17, where frequencies appear at their expected placements, while morphological characteristics remain essentially identical.

Figure 17. FFT diagram and contact point trace plot –top left– for a forced experiment. Above pattern frequency forcing. $SR = 1.25 - FR = 1.1 - LR = 0.3$.
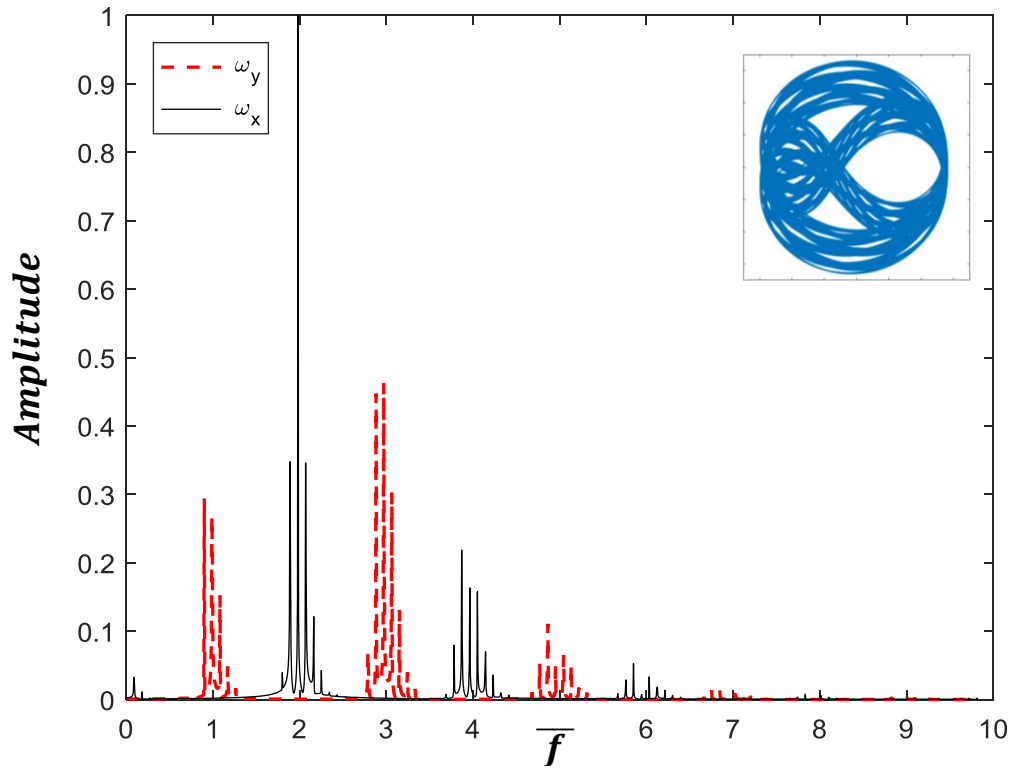
Figure 18. FFT diagram and contact point trace plot –top left– for a forced experiment. Under pattern frequency. $SR = 2.2 - FR = 0.9 - LR = 0.3$.
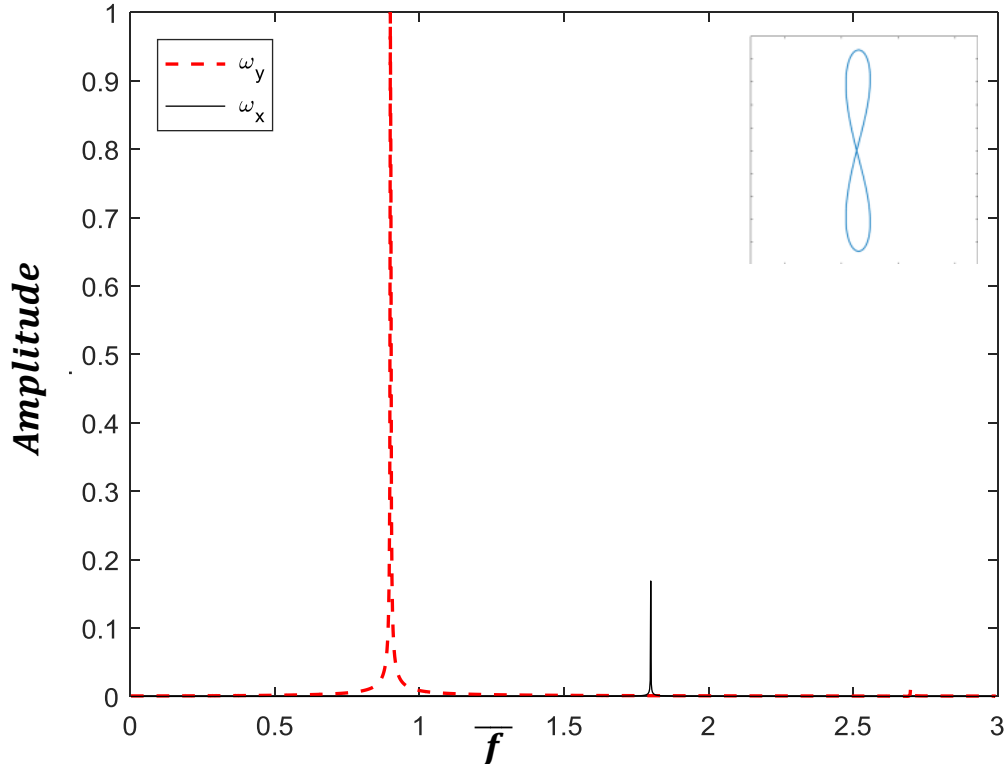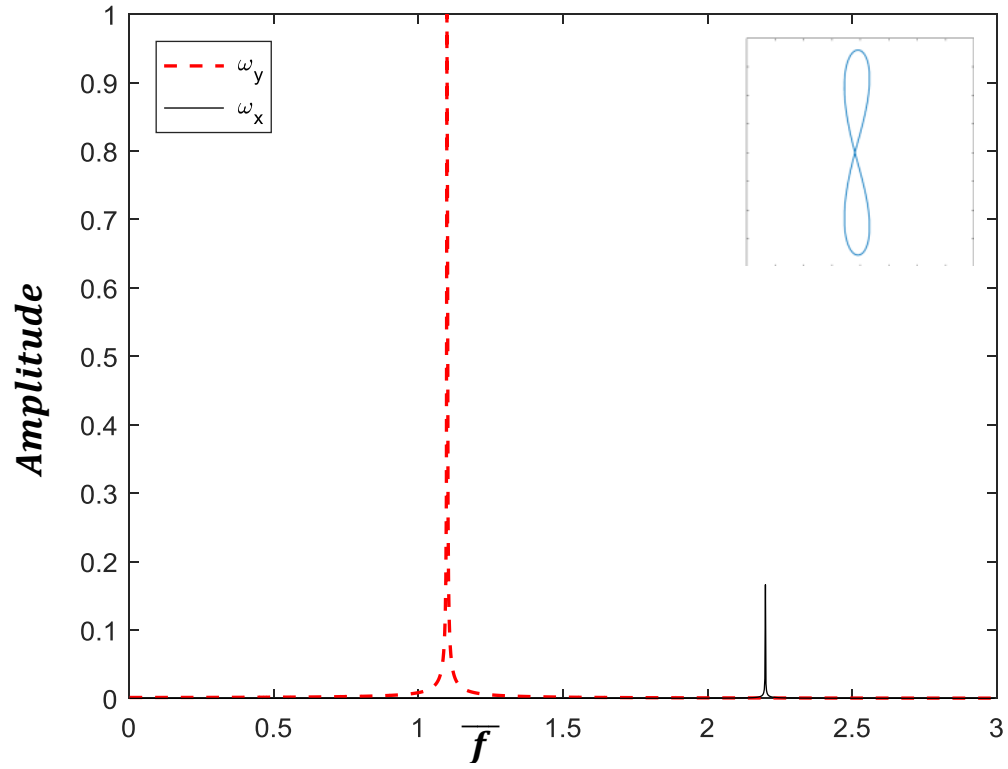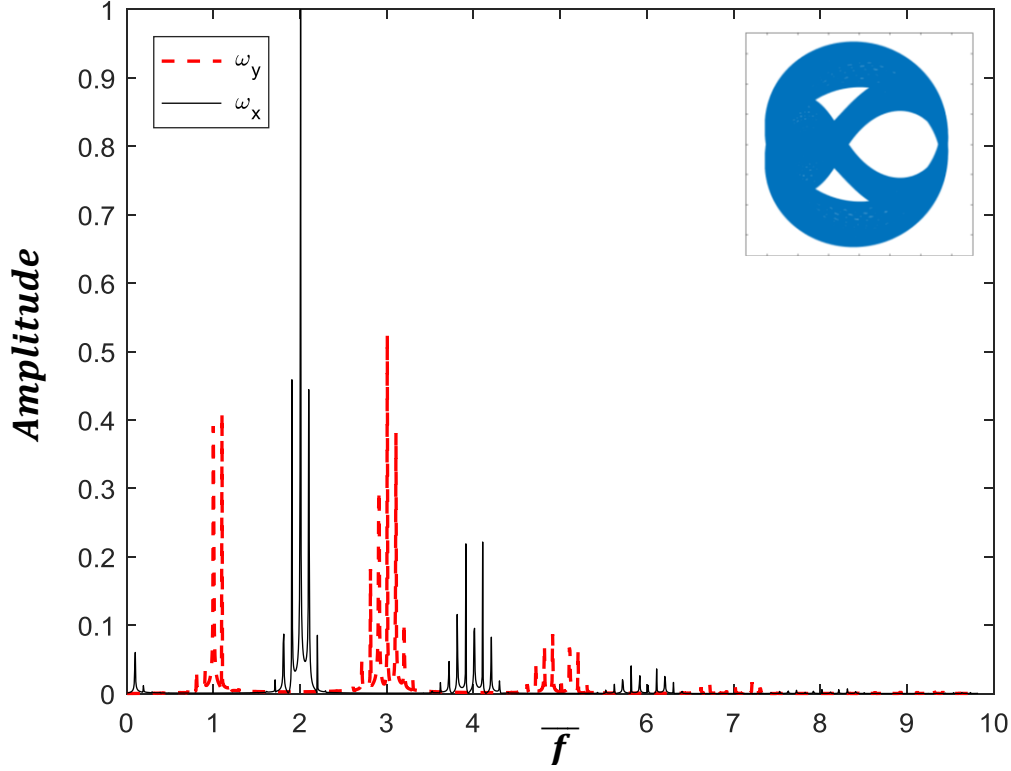
Figure 19. FFT diagram and contact point trace plot –top left– for a forced experiment. Above pattern frequency forcing. $SR = 2.2 - FR = 1.1 - LR = 0.3$.

In Figures 18 and 19, we see what can be described as a forced alternating pattern. Forcing near the pattern frequency has proved to be effective in maintaining the frequential particularities of this, more "chaotic", pattern. Forcing amplitude, while small, is now reflected on the contact point trace plots and in the own FFT diagrams, where punctual peak frequencies are now accompanied by a few secondary or residual peaks, within the same range. Apart from that, it is to be noted that there are as many main frequency peaks as found in Figure 7, disposed in a notably similar fashion, where peak position and relevancy have barely been affected by the implementation of the external forcing.

Let us remember the frequency positioning discovered in the previous chapter, that is: $\overline{f}_y^i = (2i - 1)\overline{f}_y^1$, and $\overline{f}_x^i = (2i)\overline{f}_y^1$, for $i = 1,2,3$. Now that the frequency spectrum on the y-axis is effectively normalized by the pattern frequency, it is best observed how this law is obeyed: with peaks standing on integer values.

Figure 20. FFT diagram and contact point trace plot –top left– for a forced experiment. Under pattern frequency forcing. $SR = 3.8 - FR = 0.9 - LR = 0.1$.

Figure 21. FFT diagram and contact point trace plot –top left– for a forced experiment. Under pattern frequency forcing. $SR = 3.8 - FR = 0.9 - LR = 0.3$.

Figure 22. FFT diagram and contact point trace plot –top left– for a forced experiment. Above pattern frequency forcing. $SR = 3.8 - FR = 1.1 - LR = 0.1$.

Figure 23. FFT diagram and contact point trace plot –top left– for a forced experiment. Above pattern frequency forcing. $SR = 3.8 - FR = 1.1 - LR = 0.3$.
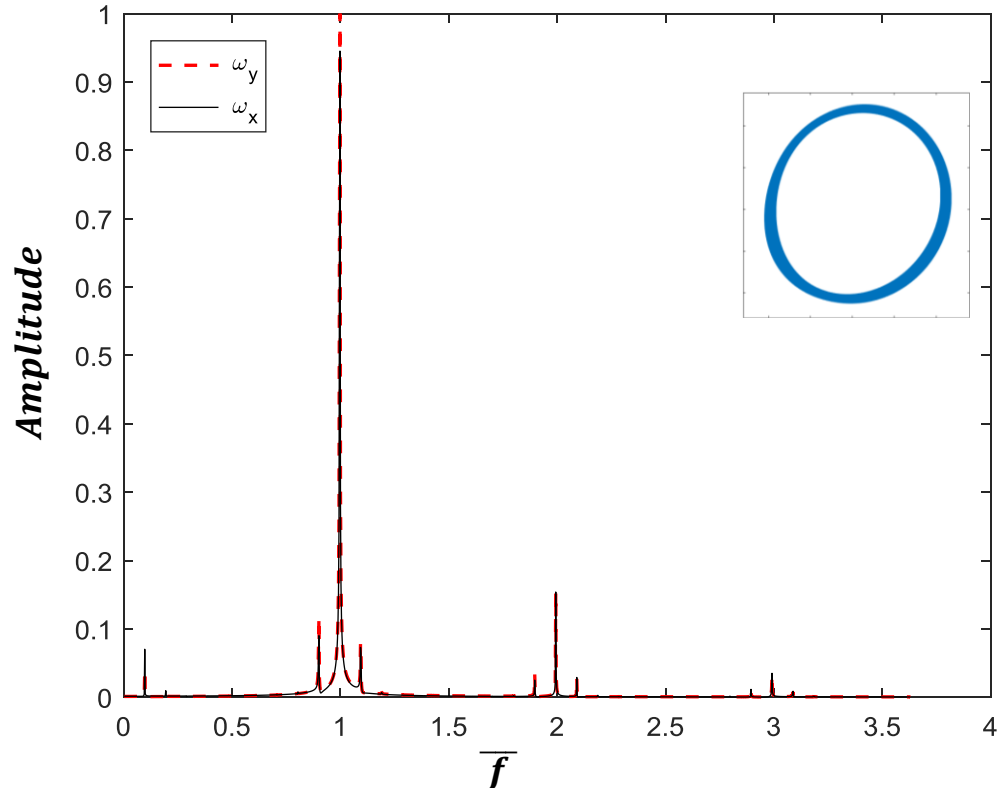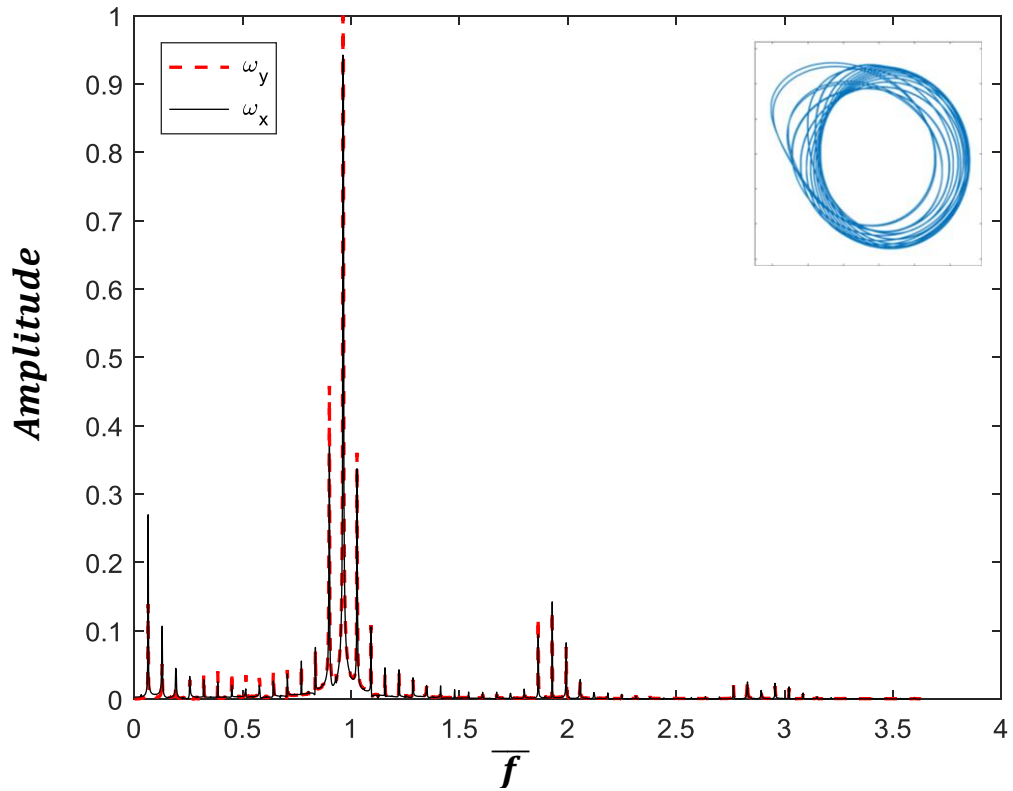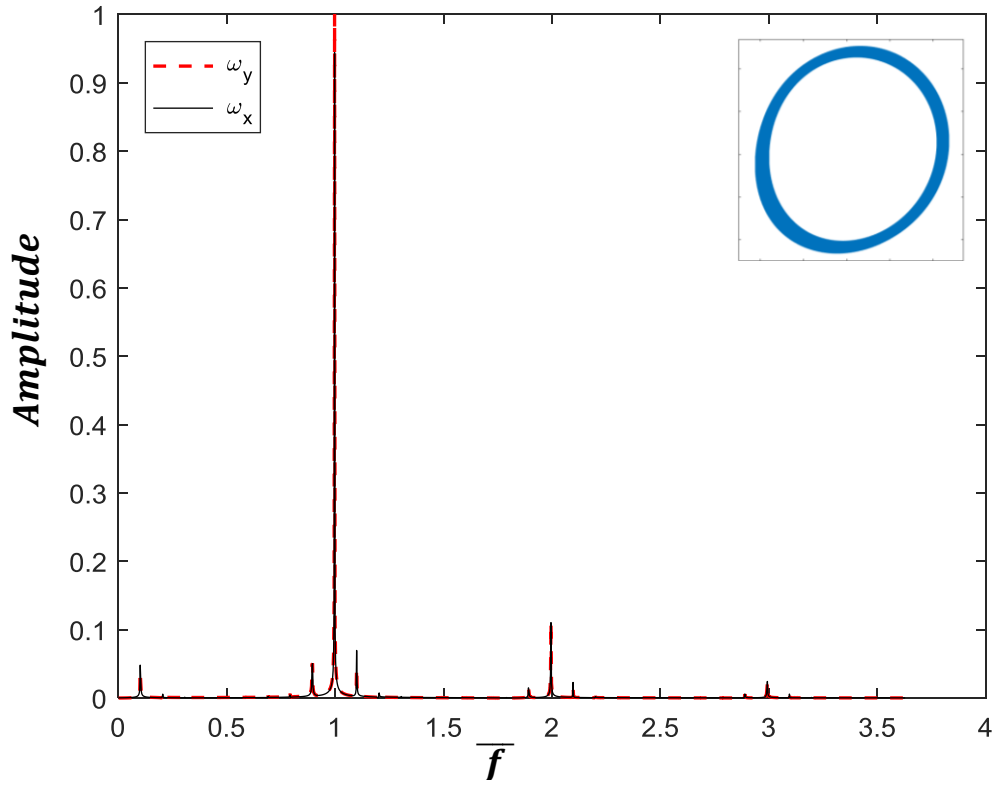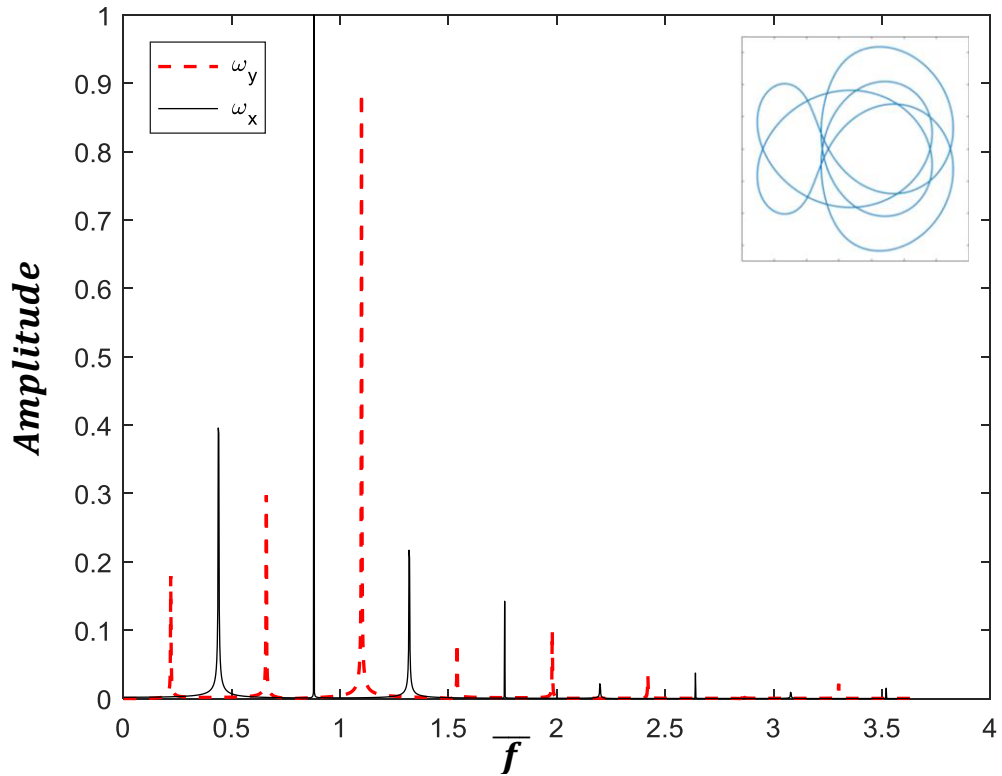
Figures 20 and 21 show the frequency response of the forced experiment to slightly under-pattern-frequency forcing with small amplitudes. Figures 22 and 23 show the frequency response of the forced experiment to slightly above-pattern-frequency forcing with small amplitudes. A total of four figures are included for this specific 3.8 speed-ratio (SR) to better understand the existence of a stability threshold, heavily correlated with a limiting length ratio –as seen in Table 3.

In Figure 20, the translated coiling morphology has remained close to the original, unforced one. The tiny forcing amplitude barely affects the overall kinematics. However, in Figure 21, we can see in the contact point trace plot how the thread deposition is not uniform anymore. It has been in fact deflected from the circular path. This irregularity appears in the FFT diagram in the form of numerous and widespread residual frequency peaks. Although hardly countable, all frequency peaks are replicated or coupled, that is, a particular –big or small– peak is both encountered for the x- and y-coordinates ($\overline{f}\,_x^{\,i} = \overline{f}\,_y^{\,i}$). Moreover, amplitude ratio is always of the order of the unity ($A^i \sim 1$).

Let us now take a look at the second pair of figures. Figure 22 reproduces a result with the same essential characteristics of Figure 20, such as moderated thread deposition displacement and compliance with translated coiling pattern frequential behavior. Residual frequency peaks are limited and only appear near the primary peaks, still in a coupled fashion. At the other extreme, Figure 23 throws up some out-of-the-box results. Firstly, the contact point trace plot is no longer of circular geometry. Instead, a series of curves of different eccentricities intersect one another at different points of the axis system. To a certain extent, thread deposition geometry somewhat resembles the original alternating pattern. Frequency analysis does actually corroborate this resemblance. Frequency peaks are no longer coupled and there are not any residual frequencies. Instead, the following law is observed: $\overline{f}\,_y^{\,i} = (2i - 1)\overline{f}\,_y^{\,1}$ and $\overline{f}\,_x^{\,i} = (2i)\overline{f}\,_y^{\,1}$. The greatest frequency peaks for both x- and y-axes are found slightly before ($\overline{f}\,_x^{\,2}$) and after ($\overline{f}\,_y^{\,3}$) the unity.

While probably obvious to the reader, it feels appropriate to clarify why a finite number of frequency peaks may or may not show in the FFT diagram. In short, the entirety of the simulations performed in this project can each be reduced to a specific periodic geometry over the belt plane. We are referring to the contact point trace plot. Sometimes larger, sometimes shorter –in size and time–, the solution of our program has been able to reproduce a unique and singular geometry adapted to the particular user-defined circumstances. The amount and diversity of simulations contained herein represent only a really small part of the complete spectrum, so it does not seem advisable to unequivocally expect this finite frequency behavior. This kind of experiments is, however, beyond the scope of this project.

5. Conclusions

The Fluid-Mechanical Sewing Machine problem has been the subject of numerous research efforts throughout the last decade, and yet an external stimulus has not been added to the equation. Previous work included in the *References* section has proved to be indispensable for the development of our new geometrical model. Advantages of understanding and controlling this type of forcing intricacies would potentially lead to the enhancement of process manufacturing or the optimization of material mechanical characteristics.

In this section we will omit judgments of the work conducted in Chapters 2-3, which consists on a mere, personalized reproduction of the work carried out by the cited professionals. Its inclusion in the present project acts as a formal introduction to the FMSM problem. It may as well serve as a way of appreciation for their phenomenal scientific contributions.

Let us then focus on the conclusions extracted from Chapter 4: *Statistical and frequency characterization of perturbed flow*. The analysis of results may be divided into two groups: in short, satisfactory and unsatisfactory results.

In the first group we may include experiments where forcing happens for what were originally meanders. As a matter of fact, forcing experiments in the surroundings of the pattern frequency for low speed ratios ($SR = 1.25$) achieved a flawless frequency scheme, with a complete lack of residual peaks. Pattern adaptation resulted excellent. Secondly, the alternating loops offered a notably adequate behavior. While forcing did become noticeable –at least in the FFT diagrams–, thread disposition over the moving belt shared the essential characteristics of the original alternating pattern, for all amplitudes and frequencies tested.

On the other side, unsatisfactory results are mainly limited to experimentation with translated coils. Simulations with high speed ratios ($SR = 3.8$) have not responded well to forcing near pattern frequency, practically independently of perturbation amplitude. The appearance of a large amount of residual frequencies, at first, leads to quasi-total disfigurement of what once had been introduced as a coil, statistically and frequentially speaking.

It is suggested by these unappealing instabilities that we exhort the reader to carefully consider each and every one of the results here seen. External circumstances have limited the scope of this project to a numerical examination of the new geometrical model. An even more complete and rigorous description of the problem should be made possible once results in this work are properly corroborated in the laboratory.

Annexes

Considerations.

→ Equation 10c captures the shape of the hanging thread as set by the balance of viscous forces and gravity:

$$\theta' = \kappa(r, \theta - \psi)$$

where

$$\kappa(r, \theta - \psi) = \frac{1}{R_c} \sqrt{\frac{r}{R_c}} \left(1 + A(\theta - \psi) \frac{r}{R_c} \right) \sin(\theta - \psi)$$

where

$$A(\theta - \psi) = \frac{b^2 \cos(\theta - \psi)}{1 - b \cos(\theta - \psi)}$$

where

$$b = 0.715$$

For more information on this fitting function, see Ref. [1].

→ For tables in Chapter 4: *Statistical and frequency characterization of perturbed flow*, the maximum amplitude is defined as follows:

$$|A|_{max} = \frac{y_{max} - \mu_y}{Rc}$$

where y_{max} is the largest y-axis value in an experiment, and μ_y is the y-axis mean.

→ The root mean square (RMS), or quadratic mean, is defined as the square root of the mean square. In the case of a set of values, such as the numerical discretization of local thread deposition over the belt plane, the following formula is utilized:

$$RMS = \sqrt{\frac{1}{n} \sum_{i=1}^{n} x_i^2}$$

where n is the total amount of values in the set, and x_i is the value of the i-th element of the set.

→ Certain limiting considerations are to be taken into account when carrying out a forced experiment:

1) Let us recover the sinusoidal forcing being implemented on our new scheme. A standard sinusoidal curve in our system may be defined as follows:

$$y(t) = A \sin \omega t \qquad x(t) = Vt$$
$$\frac{dy}{dt}(t) = A\omega \cos \omega t \qquad \frac{dx}{dt}(t) = V$$

Now let $T = \frac{2\pi}{\omega}$ be the period of the sine wave, then the arc length of the sine wave, λ_{sin}, is defined in the following manner:

$$\lambda_{sin} = \int_{0}^{\lambda_{sin}} ds = \int_{0}^{VT} \sqrt{1 + \left(\frac{dy}{dx}\right)^2} \, dx = \int_{0}^{T} \sqrt{1 + \left[\left(\frac{dy}{dt}\right)\left(\frac{dt}{dx}\right)\right]^2} \left(\frac{dx}{dt}\right) dt$$

$$= \int_{0}^{T} \sqrt{1 + \left(\frac{A\omega}{V} \cos \omega t\right)^2} \, V \, dt = \int_{0}^{T} \sqrt{1 + \left[\frac{2\pi A}{VT} \cos\left(\frac{2\pi t}{T}\right)\right]^2} \, V \, dt$$

This integral is numerically solved in MATLAB and can be compared with the actual arc length value expected, given by $\lambda = U_c T$. λ represents the total amount of material extruded within one complete wave.

These two presented length variables will not, if un-manipulated, coincide and the problem would pose a threat whenever the hypothetical length surpassed the real one, that is, $\lambda_{sin} > \lambda$. This would in effect mean that the actual extruded material within a wave would be lower than the own sine wave trajectory, which would make for an evidently not uniform thread placement over the belt.

2) In a second physical incertitude, attention is paid to speed ratio between the coiling speed and the forcing speed. Let us denote it secondary speed ratio, SR_2. The forcing speed, or average wave speed, is given by the following expression:

$$AVG\left(\left|\frac{dy}{dt}\right|\right) \equiv \hat{Y} = \frac{\Delta s}{\Delta t} = \frac{4A}{T} = 4Af_y = 4R_c LR f_p FR = 4R_c \, f_c \, LR \, FR0 \, FR = \frac{2}{\pi} U_c \, LR \, FR0 \, FR$$

where LR is the ratio between the forcing amplitude, A, and the steady coiling radius, R_c; $FR0$ is the ratio between the pattern frequency, f_p, and the steady coiling frequency, f_c; and FR is the ratio between the forcing frequency, f_y, and the pattern frequency.

When compared with the extruding speed, we obtain:

$$SR_2 = \hat{Y}/U_c = \frac{2}{\pi} LR \, FR0 \, FR$$

In a similar fashion, another problem would appear if this ratio were superior to the unity. That would effectively mean that the average wave speed would be greater than the extruding speed. In another words, not enough extruded material would ever cover the $4A$ periodic length. A lack of material is to be expected and the thread would consequently be inconsistent.

This second consideration is quantitatively more restrictive than the first condition, but it seems adequate to take both into account to better understand the physical circumstances of a user-defined simulation.

Term index.

—	A	Forcing movement amplitude.
—	A^i	Ratio of amplitudes for the spectra for $\overline{f}\,^i_x$ and $\overline{f}\,^i_y$.
—	$|A|$	Absolute punctual amplitude or deviation from the mean.
—	$[\boldsymbol{e}_x\,\boldsymbol{e}_y]$	Cartesian basis.
—	$[\boldsymbol{e}_r\,\boldsymbol{e}_\psi]$	Polar basis.
—	f_c	Steady coiling frequency.
—	f_p	Pattern frequency.
—	f_y	Forcing movement frequency.
—	$\overline{f}$	Dimensionless frequency, normalized by f_c [Figures 6-8] or f_p [Figures 16-23].
—	$\overline{f}\,^i_x$	i-th dimensionless frequency of x-coordinate.
—	$\overline{f}\,^i_y$	i-th dimensionless frequency of y-coordinate.
—	$FMSM$	Fluid Mechanical Sewing Machine, referred by [2].
—	FFT	Fast Fourier Transform.
—	FR	Frequency ratio (f_y/f_p).
—	$FR0$	Primitive frequency ratio (f_p/f_c).
—	ϕ	Direction of the tangent relative to the line joining the projection of the nozzle O to the point of contact $\boldsymbol{r}$.
—	GM	Geometrical Model, as described by [1].
—	κ	Curvature of the thread.
—	$LM2$	Laboratory for Multiscale Mechanics, research group from École Polytechnique de Montréal.
—	LR	Length ratio (A/R_c).
—	λ	Amount of material extruded within a periodic forcing wave.
—	λ_c	Amount of material extruded within a steady coiling cycle.
—	λ_p	Amount of material extruded within a pattern cycle.
—	λ_{sin}	Virtual arc wave length carried out under the juxtaposition of x and Y.
—	NGM	New Geometrical Model, described in Chapter 2: *Physics of the new geometrical model*.
—	O	Projection of the nozzle over the belt at $y=0$.
—	ψ	Angular coordinate of the polar frame of reference.
—	$\boldsymbol{q}$	Position on the belt of the point s at time t.
—	$\boldsymbol{r}$	Point of contact of the thread on the belt.
—	r	Radial coordinate of the polar frame of reference.

—	R_c	Steady coiling radius.
—	RMS	Root mean standard.
—	s	Arc length along the trace.
—	SR	Speed ratio (U_c/V).
—	SR_2	Secondary speed ratio ($\hat{Y}/U_c$).
—	$\boldsymbol{t}$	Unit tangent to the thread at the point of contact $\boldsymbol{r}$.
—	T_p	Pattern period.
—	T_c	Steady coiling period.
—	T	Forcing movement period.
—	θ	Angle from the x-axis to the tangent $\boldsymbol{t}$.
—	U_c	Extruding speed. Also referred to as coiling speed.
—	V	Belt speed.
—	x	Longitudinal coordinate of particular-point-in-thread position on the belt, determined by its horizontal distance to O.
—	$\widetilde{X}$	x-coordinate normalized by R_c. Used indistinctly for contact point trace plots and deposited trace plots.
—	y	Transverse coordinate of particular-point-in-thread position on the belt, determined by its vertical distance to O.
—	Y	Transverse position of the nozzle projected onto the platform. Sinusoidal function.
—	$\hat{Y}$	Average forcing movement speed.
—	$\widetilde{Y}$	x-coordinate normalized by R_c. Used indistinctly for contact point trace plots and deposited trace plots.
—	ω	Forcing movement angular speed.

MATLAB code.

```
%% ----------------------------- GENERAL --------------------------------

global Rc SR Uc Ay lambda

SR = 1.15;                              % Speed ratio.
FR = 0.3;                               % Frequency ratio.
LR = 4;                                 % Length ratio.

fc = 1;                                 % Steady coiling frequency.
Rc = 1;                                 % Steady coiling radius.
Uc = 2*pi*fc*Rc;                        % Steady coiling speed.

V = Uc/SR;                              % Belt speed.


%% ----------------------- NO FORCING PART (-0-) -----------------------

tspan = 0:1e-3:1e3;                     % Temporal integration interval.
Y_0 = [1 0 pi/2];                       % Initial conditions.

% ODE options.
options = odeset('RelTol', 1e-6, 'AbsTol', [1e-5 1e-5 1e-5], 'refine', 5);

% ODE numerical resolution - NO FORCING.
[t,Y0] = ode23(@noforcing, tspan, Y_0, options);

X10 = Y0(:,1).*cos(Y0(:,2));            % x-coordinate contact point trace.
X20 = X10 + V.*(t(end) - t);           % x-coordinate deposited trace.

Y10 = Y0(:,1).*sin(Y0(:,2));           % y-coordinate contact point trace.
Y20 = Y10;                             % y-coordinate deposited trace.

% Cutting solution array allows us to work on the steady spectrum.
n = round(length(Y0)*0.5):length(Y0);
m = round(length(Y0)*0.9):length(Y0);

% Plot of contact point trace. x- and y-coordinates are normalized by Rc.
XF10 = X10(n);
YF10 = Y10(n);
figure(1)
plot(XF10/Rc,YF10/Rc)

% Plot of deposited trace. x- and y- coordinates are normalized by Rc.
XF20 = X20(m);
YF20 = Y20(m);
figure(2)
plot(XF20/Rc,YF20/Rc)

tF = t(n);                             % Time interval.
```

```matlab
L = ceil(Uc*(tF(end) - tF(1))/Rc);     % FFT signal length.
if mod(L,2) ~= 0                        % 'If' makes signal length even.
    L = L+1;
end

% FFT on y-coordinate.
TFY0 = fft(YF10);
P2Y0 = abs(TFY0);
P1Y0 = P2Y0(1:L/2+1);
P1Y0(2:end-1) = 2*P1Y0(2:end-1);
P1Y0 = P1Y0(2:end);                     % Frequency amplitude: y-coordinate.

% FFT on x-coordinate
TFX0 = fft(XF10);
P2X0 = abs(TFX0);
P1X0 = P2X0(1:L/2+1);
P1X0(2:end-1) = 2*P1X0(2:end-1);
P1X0 = P1X0(2:end);                     % Frequency amplitude: x-coordinate.

% Frequency spectrum -normalized by coiling frequency.
f0 = 2*pi*(0:L/2)/L;
f0 = f0(2:end);

% Normalization of amplitudes by max value.
P1X0_n = P1X0/max([P1X0;P1Y0]);
P1Y0_n = P1Y0/max([P1X0;P1Y0]);

% FFT plot - NO FORCING.
figure(3)
plot(f0,P1Y0_n,'r—-','linewidth',1.25)
hold on
plot(f0,P1X0_n, 'k')
legend(' \omega_y',' \omega_x','location','northwest')
xlabel('\omega')
ylabel('Amplitude')
hold off

% 'while' loop finds the first characteristic y-frequency peak on the
% normalized frequency spectrum, known as pattern frequency. RMS value is used
% as level indicator.
i = 1;
while P1Y0_n(i) < rms(P1Y0_n)
    i = i + 1;
end
j = i;
while P1Y0_n(j) > rms(P1Y0_n)
    j = j + 1;
end
[A,B] = max(P1Y0_n(i-1:j));             % A: max value. B: max value position.
FR0 = f0(i+B-2);                        % Normalized pattern frequency.
fp = fc*FR0;                            % Pattern frequency.
```

```matlab
%% --------------------------- FORCING PART -------------------------------

fy = fp*FR;                          % Forcing movement frequency.
Ay = Rc*LR;                          % Forcing movement amplitude.

lambda = Uc/fy;                      % Total amount of material extruded.
                                     % within a perturbation cycle.
% ODE numerical resolution – FORCING.
[t,Y] = ode23(@forcing, tspan, Y_0, options);

Yc = Ay*sin(2*pi*Uc*t/lambda);       % Sinusoidal forcing function.

X1 = Y(:,1).*cos(Y(:,2));            % x-coordinate contact point trace.
X2 = X1 + V.*(t(end) - t);           % x-coordinate deposited trace.

Y1 = Y(:,1).*sin(Y(:,2)) + Yc;       % y-coordinate contact point trace.
Y2 = Y1;                             % y-coordinate deposited trace.

% Plot of contact point trace. x- and y-coordinates are normalized by Rc.
XF1 = X1(n);
YF1 = Y1(n);
figure(4)
plot(XF1/Rc,YF1/Rc)

% Plot of deposited trace. x- and y-coordinates are normalized by Rc.
XF2 = X2(m);
YF2 = Y2(m);
figure(5)
plot(XF2/Rc,YF2/Rc)

% FFT on y-coordinate.
TFY = fft(YF1);
P2Y = abs(TFY);
P1Y = P2Y(1:L/2+1);
P1Y(2:end-1) = 2*P1Y(2:end-1);
P1Y = P1Y(2:end);                    % Frequency amplitude: y-coordinate.

% FFT on x-coordinate.
TFX = fft(XF1);
P2X = abs(TFX);
P1X = P2X(1:L/2+1);
P1X(2:end-1) = 2*P1X(2:end-1);
P1X = P1X(2:end);                    % Frequency amplitude x-coordinate.

% Frequency spectrum normalized by pattern frequency.
f = f0/FR0;

% Normalization of amplitudes by max value.
P1X_n = P1X/max([P1X;P1Y]);
P1Y_n = P1Y/max([P1X;P1Y]);

% FFT plot - EXTERNAL FORCING
```

```matlab
figure(6)
plot(f,P1Y_n,'r—-','linewidth',1.25)
hold on
plot(f,P1X_n,'k')
legend(' \omega_y',' \omega_x','location','northwest')
xlabel('omega')
ylabel('Amplitude')
hold off


%% ---------------------- LIMITING CONSIDERATIONS ------------------------
%% 1) EXTRUDED MATERIAL AND SINE WAVE TRAJECTORY

fun = @(t) V*sqrt(1+(2*pi*Ay*fy/V*cos(2*pi*fy*t)).^2);
lambda2 = integral(fun,0,1/fy);         % Regular sine wave arc length

if lambda2 > lambda
      status = 'WARNING: E < lambda';
else
      status = '-';
end

%% 2) EXTRUDING SPEED AND PERTURBATION SPEED

if LR*FR*FR0 > pi/2
      status2 = 'WARNING: Uc < Uw';
else
      status2 = '-';
end


%% ------------------------- CALLED FUNCTIONS ----------------------------

% No-forcing ODE.
function dY = noforcing(t,Y)            % Y(1) = r, Y(2) = phi, Y(3) = theta

global Rc SR Uc
dY = zeros(3,1);
b = 0.715;
A = b^2 * cos(Y(3)-Y(2)) / (1 - b*cos(Y(3)-Y(2)));
kappa = sqrt(Y(1)/Rc^3) * (1 + A*Y(1)/Rc) * sin(Y(3)-Y(2));

dY(1) = Uc*cos(Y(3)-Y(2)) + V*cos(Y(2)));
dY(2) = (Uc*sin(Y(3)-Y(2)) - V*sin(Y(2))) / Y(1);
dY(3) = Uc*kappa;
end

% Forcing ODE.
function dY = forcing(t,Y)

global Rc SR Uc Ay lambda
```

```
dY = zeros(3,1);
b = 0.715;
A = b^2 * cos(Y(3)-Y(2)) / (1 - b*cos(Y(3)-Y(2)));
kappa = sqrt(Y(1)/Rc^3) * (1 + A*Y(1)/Rc) * sin(Y(3)-Y(2));

u = (2*pi*Ay/lambda)*Uc;

dY(1) = Uc*cos(Y(3)-Y(2)) + V*cos(Y(2)) – u*cos(u*t/Ay)*sin(Y(2)));
dY(2) = (Uc*sin(Y(3)-Y(2)) - V*sin(Y(2)) – u*cos(u*t/Ay)*cos(Y(2)))/ Y(1);
dY(3) = Uc*kappa;
end
```

References

 [1] Brun, P.-T., Audoly, B., Ribe, N. M., Eaves, T. S., and Lister, J. R., 2015, "Liquid Ropes: A Geometrical Model for Thin Viscous Jet Instabilities," Phys. Rev. Lett., 114, p. 174501.

[2] Chiu-Webster, S., and Lister, J., 2006, "The Fall of a Viscous Thread Onto a Moving Surface: A Fluid-Mechanical Sewing Machine," J. Fluid Mech., 569, pp. 89–111.

[3] Passieux, R., Guthrie, L., Rad, S. H., Lévesque, M., Therriault, D., and Gosselin, F. P., 2015, "Instability-Assisted Direct Writing of Microstructured Fibers Featuring Sacrificial Bonds," Adv. Mater., 27(24), pp. 3676–3680.

[4] Zou, S., Therriault, D. and Gosselin F. P., 2018, "Failure mechanisms of coiling fibers with sacrificial bonds made by instability-assisted fused deposition modeling," *Soft Matter*, 2018, 14, 9777.

[5] Jawed, Mohammad K.; Brun, Pierre-Thomas and Reis, Pedro M. "A Geometric Model for the Coiling of an Elastic Rod Deployed Onto a Moving Substrate." Journal of Applied Mechanics 82, 12 (December 2015): 121007.